Finite Difference Analysis of Rotationally Symmetric Shells Under Discontinuous Distributed Loadings

Troy Alvin Smith*
U.S. Army Missile Command, Redstone Arsenal, Alabama

Most published procedures for finite-difference analysis of shells indicate that analysis for discontinuous loadings must be accomplished by segmenting the shell at points of loading discontinuities. Other procedures, notably the finite-difference energy method, use a finite-difference mesh for which the tangential and transverse nodal points are staggered to obtain satisfactory solutions. This results in incompatibility of transvere displacements and rotations at the tangential nodal points. It is shown here that correctly coverging solutions with full compatibility of displacements and derivatives may be obtained for either continuous or discontinuous loadings without segmenting the shell at loading discontinuities. This has been achieved by formulating the differential equations of equilibrium directly in terms of the displacements, by using an ordinary finite-difference representation of the derivatives, and by using a nodal point mesh, which includes all displacement components at every point in the mesh and does not include the points of loading discontinuities. It has also been demonstrated, with results not shown here, that this correct solution convergence without segmenting the shell meridian is not obtainable for all differential equation formulations and finite-difference representations. Time-dependent natural boundary conditions may be imposed at the shell boundaries, and Fourier series representations have been used for all loadings and dependent variables in the circumferential direction of the shell. To complete system of finite-difference equations is solved implicitly for the first time increment, while an explicit solution for variables within the boundary edges of the shell, together with separate implicit solutions at each boundary, is used for subsequent time increments. Solutions obtained for a cylindrical shell under static discontinuous loadings without segmenting the shell meridian have been included and are shown to agree with solutions obtained by segmenting the shell meridian. Static solutions for a parabolic shell under discontinuous loadings have also been compared with solutions found by a well-known finite-element program and are shown to be in agreement with the finite-element solutions.

Nomenclature

$A_1,\ldots,A_{10}$ = parameters used in Eq. (23) and defined in Ref. 14
$B_1,\ldots,B_{13}$ = parameters used in Eq. (24) and defined in Ref. 14
C = coefficients of the force variables $N_{\phi n}$, $M_{\phi\psi}$, N_n, and Q_n in the finite-difference equations obtained before change of force variables
C^0 = coefficients of the modified force variables $N^0_{\phi n}$, $M^0_{\phi n}$, N^0_n, and Q^0_n in the governing finite-difference equations
$C_1,\ldots,C_9$ = parameters used in Eq. (25) and defined in Ref. 14
D = flexural rigidity of shell, $=Eh^3/12(1-\nu^2)$
$D_1,\ldots,D_{50}$ = parameters used in Eqs. (27-32) and defined in Ref. 14
E = Young's modulus
g = acceleration constant
h = thickness of the shell
K = extensional rigidity of the shell, $=Eh/(1-\nu^2)$
m_θ,m_ϕ = moments of the mechanical surface loads
$M_\theta,M_\phi,M_{\theta\phi}$ = moment stress resultants
$M^0_{\phi n}$ = $M_{\phi n}\times 10^{-6}$
n = integer, which designates the nth Fourier component
N,Q = effective shear resultants
N^0_n,Q^0_n = $N_n\times 10^{-6}$ and $Q_n\times 10^{-6}$, respectively
$N_\theta,N_\phi,N_{\theta\phi}$ = membrane stress resultants
$N^0_{\phi n}$ = $N_{\phi n}\times 10^{-6}$
p,p_θ,p_ϕ = components of the mechanical surface loads
Q_θ,Q_ϕ = transverse shear resultants
r = distance of the point on the middle surface of the shell from the axis of symmetry
R_θ,R_ϕ = principle radii of curvature of the middle surface of the shell
s = distance from an arbitrary origin along the meridian of the shell in the positive direction of ϕ
Δs = increment of the space variable s
s_0 = value of the coordinate s at the boundary s_0, denoted also as the boundary z_0, of the shell
s_N = value of the coordinate s at the boundary s_N, denoted also as the boundary z_N, of the shell
s_i = point on the meridional line of the shell at station i, where i varies consecutively from $i=-2$ to $N+2$
t = independent time variable
Δt = increment of the time variable t
t_0 = initial value of the time variable t
t_1 = value of the time variable one time increment after time t_0
T,T_0,T_1 = temperature increment and temperature resultants
u_θ,u_ϕ,w = components of displacement of the middle surface of the shell
$\dot{u}_\theta,\dot{u}_\phi,\dot{w}$ = components of velocity of the middle surface of the shell
z = distance of any point on the middle surface of the shell measured from the origin along the axis of symmetry
z_0 = value of the coordinate z at the boundary z_0, denoted also as the boundary s_0, of the shell

Submitted March 21, 1984; revision submitted April 13, 1987.

*Aerospace Engineer.

z_N = value of the coordinate z at the boundary z_N, denoted also as the boundary s_N, of the shell
α = coefficient of thermal expansion of shell material
β_θ, β_ϕ = angles of rotation of the normal to the middle surface of the shell
γ = weight of shell material per unit volume
θ, ϕ, ρ = coordinates of any point of the shell
μ = parameter used in Eq. (44) to select an increment Δt
ν = Poisson's ratio
ω = circular frequency of vibration of the shell, rad/s
ω_{max} = highest calculated circular frequency of vibration of the shell

Introduction

A SIGNIFICANT number of reports describing differential equation formulations and accompanying finite-difference representations for solution of the rotationally symmetric shell problem appear in the literature. The authors of these reports include: Penny,[1] who solved the symmetric bending problem of a general shell in 1961; Radkowski et al.,[2] who presented solutions for the axisymmetric static problem in 1962; Budiansky and Radkowski,[3] who solved the unsymmetrical static bending problem in 1963; and Johnson and Greif,[4] who presented solutions for the dynamic response of a circular cylindrical shell with constant geometric and material properties in 1966.

Further reports include that by Bushnell,[5] who published methods for the analysis of buckling and vibration of ring-stiffened segmented shells of revolution in 1970; by Smith,[6] who published finite-difference procedures for analysis of rotationally symmetric general shells under either static or time-dependent loadings in 1971; by Greenbaum and Cappelli,[7] who published a review of numerical methods to analyze shell structures in 1971; and by Anderson et al.,[8] who compared analytical methods for stress, buckling, and vibration analysis of shells of revolution in 1971. Subsequently, reports were published by Noor and Stephens,[9] who gave a comparison of finite-difference methods for analysis of shells of revolution in 1973; by Bushnell,[10] who compared the finite-difference energy method and the finite-element method for stress, buckling, and vibration analysis of shells of revolution in 1973; by Bushnell,[11,12] who published a program for buckling of elastic-plastic complex shells of revolution including large deflections and creep in 1976 and an extensive program for stress, buckling, and vibration analysis of complex shells of revolution in 1977; and by Smith,[13] who published procedures for the static and dynamic analysis of rotationally symmetric shells of revolution utilizing the displacement formulation of the differential equations in conjunction with a high-order finite-difference representation for the derivatives in 1980.

In Ref. 1, a special set of boundary conditions is used and no consideration is given to discontinuous loadings. In Refs. 2–4, the field equations are applied separately over each region of the shell that contains no loading or geometrical discontinuities. These equations are supplemented by appropriate junction conditions at the several junctions between regions and by the boundary conditions to obtain the complete system of equations.

In Ref. 5, a finite-difference energy method is used and the assumptions include the condition that the loadings are axisymmetric. The tangential displacements u_i and v_i are located midway between the transverse displacements w_i and

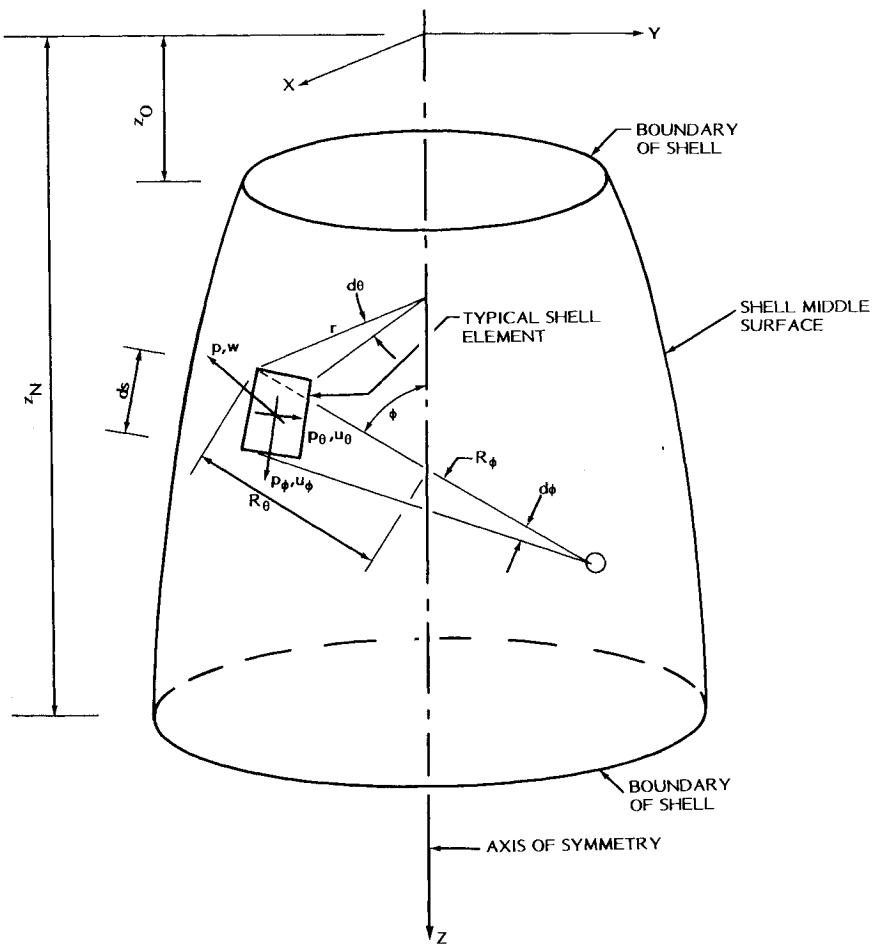

Fig. 1 Typical shell of revolution.

w_{i+1} in the finite-difference mesh. The results in incompatibility of transverse displacements and derivatives thereof at the "finite-difference element" boundaries.

In Ref. 6, the field equations consist of eight first-order partial differential equations in the space variable, and ordinary finite-difference representations are used for both spatial and time derivatives. All finite-difference equations for all fundamental variables are written at each point in the mesh, and correctly converging results are obtained for continuous loadings. Discontinuous loadings are not mentioned, but correct solutions may be obtained for those loadings only by segmenting the shell at points of loading discontinuities and applying the proper continuity conditions between shell segments.

In Ref. 7, it is stated that finite differences cannot be used at locations where the derivatives are discontinuous but that "this problem can be eliminated by application of transition or compatibility and equilibrium expressions at the discontinuities." Similarly, the authors of Ref. 8, in comparing four major programs in the article, state that each of the programs utilizes segmentation of the structure to accommodate loading discontinuities.

The study conducted in Ref. 9, with primary attention directed to finite-difference schemes used in conjunction with a first-order differential equation formulation of the governing equations, did not consider the case of discontinuous loadings. However, we do not generally expect correct solutions for discontinuous loadings with a first-order differential equation formulation without segmenting the shell at points of loading discontinuities.

In Refs. 10–12, the finite-difference energy method is again used, with the tangential displacements u_i and v_i occurring midway between the transverse displacements w_i and w_{i+1}. This results in a "finite-difference element," which is incompatible in normal displacements and derivatives thereof at element boundaries. In Ref. 10, several finite-element and finite-difference discretization techniques are discussed. It is stated therein that, for the "finite-difference element" in which the displacements u_i, v_i, and w_i are given at the same point and the integration areas for membrane and bending energy are the same, numerical results were unsuccessful and that discontinuities may exist for all variables at element boundaries.

In Ref. 13, the field equations are formulated in terms of the displacements, and higher-order finite-difference representations are used for the derivatives. Correctly converging results are obtained for continuous loadings by writing all equations for all fundamental variables at each point in the mesh. Discontinuous loadings have not been considered, but correct solutions for these loadings cannot be obtained without segmenting the shell at points of loading discontinuities and applying proper continuity conditions between shell segments.

The purpose of this article is to present a differential equation formulation and finite-difference representation for the derivatives, which achieves compatibility of all displacement components and derivatives thereof at all points in the finite-difference mesh and does not require shell segmentation at points of loading discontinuities. This has been achieved by formulating the differential equations of equilibrium directly

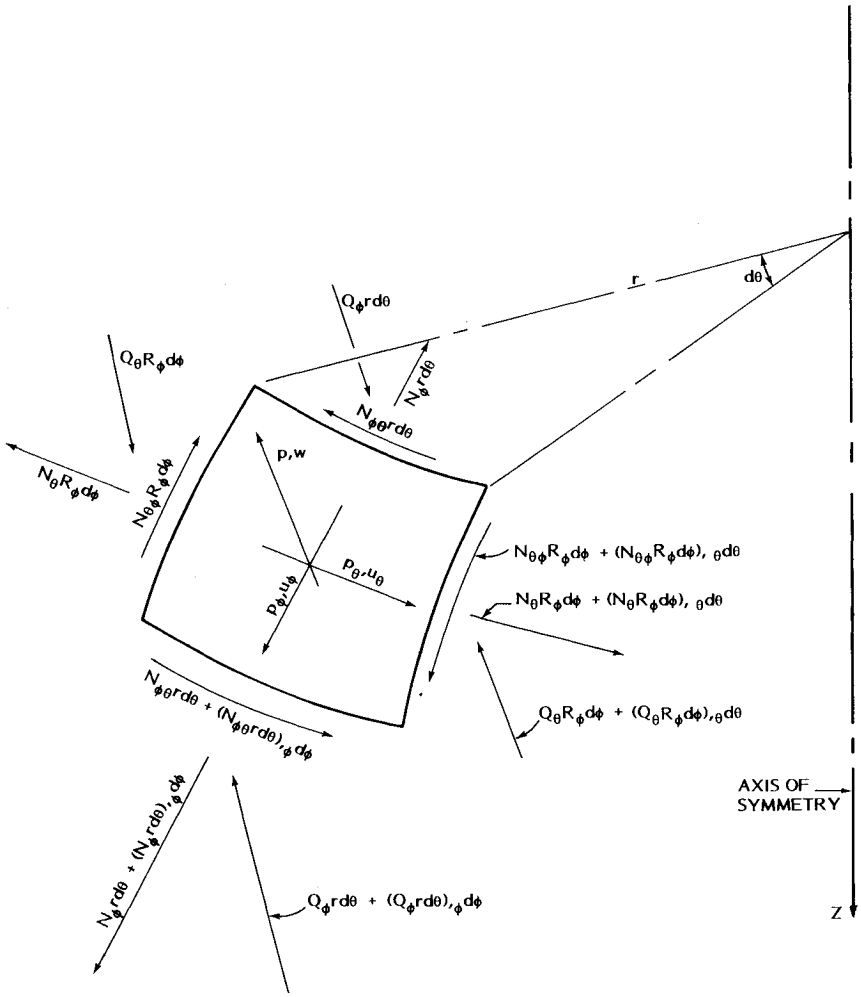

Fig. 2 Shell element membrane and shear forces.

in terms of the displacements, by using an ordinary finite-difference representation of the derivatives, and by using a nodal point mesh which includes all displacement components at every point in the mesh and does not include the points of loading discontinuities.

It has been found numerically for numerous example cases for many types of shells that solutions obtained with this formulation and finite-difference representation are the same solutions as obtained by segmenting the shell at points of loading discontinuities and that correct solutions as close as we wish at the points of loading discontinuities may be obtained by choosing the meridional increment to be sufficiently small. The rationale for expecting these numerical results for the formulation and finite-difference representations used and for expecting unsatisfactory results for certain other formulations and finite-difference representations without segmenting the shell will be presented following the example numerical results.

Governing Differential Equations

The development of our governing differential equations is fully described in Ref. 13 and given more completely in Ref. 14. However, to provide convenient reference, included in this development is a brief description and listing of those equations. Although any shell theory could be used, our system of equations is based upon the linear classical theory of shells as given by Reissner.[15] Surface loadings and inertial forces in the coordinate directions w, u_ϕ, and u_θ will be considered. The thickness h of the shell may vary along the meridian, and we assume continuity of h and its derivatives through the second order. We assume that $\rho/R_\phi \ll 1$ and $\rho/R_\theta \ll 1$. Hence, we take $N_{\theta\phi}=N_{\phi\theta}$ and $M_{\theta\phi}=M_{\phi\theta}$.

The geometry and coordinate system for the middle surface of our shell are shown in Fig. 1. Shell element membrane and shear forces are shown in Fig. 2, and shell element bending and twisting moments are shown in Fig. 3. The function $r=r(z)$ defines the geometry of the middle surface, but we will develop our equations with the meridional coordinate s as an independent variable. The principal radii of curvature of the middle surface may be expressed as

$$R_\phi=\frac{-[1+(r_{,z})^2]^{3/2}}{r_{,zz}} \tag{1}$$

$$R_\theta=r[1+(r_{,z})^2]^{1/2} \tag{2}$$

The required derivatives of R_ϕ with respect to the coordinate s are given in Ref. 14. The temperature resultants are, in accordance with Ref. 13, given by

$$T_0(\theta,s,t)=\frac{1}{h}\int_{-h/2}^{h/2} T(\theta,s,\rho,t)\,\mathrm{d}\rho \tag{3}$$

$$T_1(\theta,s,t)=\frac{12}{h^3}\int_{-h/2}^{h/2} \rho T(\theta,s,\rho,t)\,\mathrm{d}\rho \tag{4}$$

For simplicity, we assume that

$$E=\text{const}, \quad \nu=\text{const}, \quad \alpha=\text{const} \tag{5}$$

From two of our five useful equations of equilibrium for a typical element of the shell, we find the shear resultants Q_ϕ

Fig. 3 Shell element bending and twisting moments.

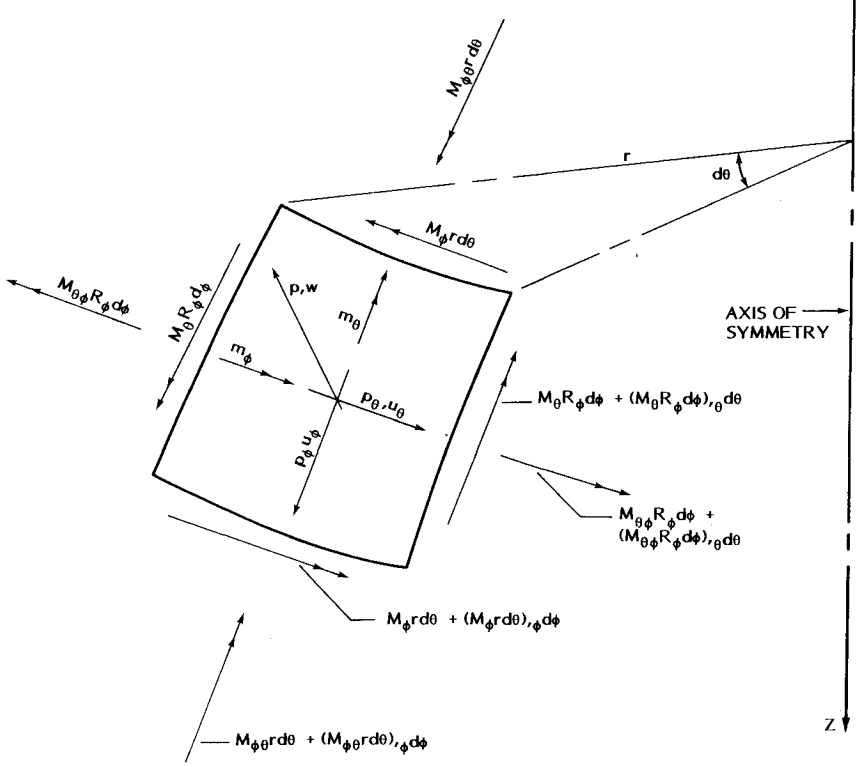

and Q_θ to be

$$Q_\phi = \frac{1}{r} M_{\theta\phi,\theta} + M_{\phi,s} + \frac{\cos\phi}{r}(M_\phi - M_\theta) + m_\phi \tag{6}$$

$$Q_\theta = \frac{1}{r} M_{\theta,\theta} + M_{\theta\phi,s} + \frac{2\cos\phi}{r} M_{\theta\phi} + m_\theta \tag{7}$$

By substituting Eqs. (6) and (7) into the remaining three equations of equilibrium, we find our three field equations to be

$$N_{\theta\phi,\theta} + rN_{\phi,s} + (N_\phi - N_\theta)\cos\phi + \frac{1}{R_\phi} M_{\theta\phi,\theta} + \frac{r}{R_\phi} M_{\phi,s} + \frac{\cos\phi}{R_\phi}(M_\phi - M_\theta) + r\left(\frac{m_\phi}{R_\phi} + p_\phi\right) - \frac{\gamma hr}{g} u_{\phi,tt} = 0 \tag{8}$$

$$\frac{1}{r} M_{\theta,\theta\theta} + 2M_{\theta\phi,\theta s} + \frac{2\cos\phi}{r} M_{\theta\phi,\theta} + rM_{\phi,ss} + 2\cos\phi M_{\phi,s} - \frac{\sin\phi}{R_\phi}(M_\phi - M_\theta) - \cos\phi M_{\theta,s} - N_\theta \sin\phi - \frac{r}{R_\phi} N_\phi + r(m_{\phi,s} + p) + \cos\phi m_\phi + m_{\theta,\theta} - \frac{\gamma hr}{g} w_{,tt} = 0 \tag{9}$$

$$N_{\theta,\theta} + rN_{\theta\phi,s} + 2\cos\phi N_{\theta\phi} + \frac{\sin\phi}{r} M_{\theta,\theta} + \sin\phi M_{\theta\phi,s} + \frac{2\sin\phi\cos\phi}{r} M_{\theta\phi} + \sin\phi m_\theta + rp_\theta - \frac{\gamma hr}{g} u_{\theta,tt} = 0 \tag{10}$$

The stress resultants in terms of the displacements w, u_ϕ, and u_θ are

$$N_\theta = K\left[\frac{1}{r}(u_{\theta,\theta} + u_\phi \cos\phi + w\sin\phi) + \nu\left(u_{\phi,s} + \frac{w}{R_\phi}\right)\right] - (1+\nu)\alpha K T_0 \tag{11}$$

$$N_\phi = K\left[u_{\phi,s} + \frac{w}{R_\phi} + \frac{\nu}{r}(u_{\theta,\theta} + u_\phi\cos\phi + w\sin\phi)\right] - (1+\nu)\alpha K T_0 \tag{12}$$

$$N_{\theta\phi} = \frac{(1-\nu)K}{2}\left[\frac{1}{r}(u_{\phi,\theta} - u_\theta\cos\phi) + u_{\theta,s}\right] \tag{13}$$

$$M_\theta = D\left[-\frac{1}{r^2} w_{,\theta\theta} + \frac{\sin\phi}{r^2} u_{\theta,\theta} + \frac{\cos\phi}{r}\left(-w_{,s} + \frac{1}{R_\phi} u_\phi\right) + \nu\left(-w_{,ss} + \frac{1}{R_\phi} u_{\phi,s} - \frac{1}{R_\phi^2} R_{\phi,s} u_\phi\right)\right] - (1+\nu)\alpha D T_1 \tag{14}$$

$$M_\phi = D\left[-w_{,ss} + \frac{1}{R_\phi} u_{\phi,s} - \frac{1}{R_\phi^2} R_{\phi,s} u_\phi + \frac{\nu}{r}\left(-\frac{1}{r} w_{,\theta\theta} + \frac{\sin\phi}{r} u_{\theta,\theta} - \cos\phi w_{,s} + \frac{\cos\phi}{R_\phi} u_\phi\right)\right] - (1+\nu)\alpha D T_1 \tag{15}$$

$$M_{\theta\phi} = \frac{(1-\nu)D}{2r}\left[-2w_{,\theta s} + \frac{2\cos\phi}{r} w_{,\theta} + \frac{1}{R_\phi} u_{\phi,\theta} + \sin\phi u_{\theta,s} + \left(\frac{\cos\phi}{R_\phi} - \frac{2\sin\phi\cos\phi}{r}\right) u_\theta\right] \tag{16}$$

The effective shear resultants N and Q are

$$N = N_{\theta\phi} + \frac{\sin\phi}{r} M_{\theta\phi} \tag{17}$$

$$Q = Q_\phi + \frac{1}{r} M_{\theta\phi,\theta} \tag{18}$$

The rotations of the normals to the middle surface are

$$\beta_\phi = -\frac{1}{R_\phi} w_{,\phi} + \frac{1}{R_\phi} u_\phi \tag{19}$$

$$\beta_\theta = -\frac{1}{r} w_{,\theta} + \frac{\sin\phi}{r} u_\theta \tag{20}$$

We obtain our three field equations in terms of the displacements w, u_ϕ, and u_θ by substituting the stress resultants defined by Eqs. (11-16) together with their appropriate derivatives into Eqs. (8-10). These equations may be found in Ref. 14.

The natural boundary values at each edge of the shell are the eight primary variables consisting of the four generalized displacements w, u_ϕ, u_θ, and β_ϕ and the four generalized forces Q, N_ϕ, N, and M_ϕ. To incorporate the boundary values β_ϕ, Q, N_ϕ, N, and M_ϕ into our system of equations as variables at the boundaries, we supplement the three field equations in terms of the displacements w, u_ϕ, and u_ϕ by writing Eqs. (19), (18), (12), (17), and (15) for β_ϕ, Q, N_ϕ, N, and M_ϕ, respectively, at each boundary in terms of the displacements w, u_ϕ, and u_θ. The three field equations together with the definition of β_ϕ, Q, N_ϕ, N, and M_ϕ at each boundary will be solved in conjunction with the equations defining the boundary conditions and the initial conditions. For the boundary conditions, we will prescribe the appropriate four of the quantities w, u_ϕ, u_θ, β_ϕ, Q, N_ϕ, N, and M_ϕ at each boundary.

Typical boundary conditions and the initial conditions are given by Eqs. (21) and (22), respectively, of Ref. 13.

To solve the system of equations, we expand all loadings and dependent variables in the circumferential direction of the shell in truncated Fourier series.

The Fourier series representations of the loadings p_ϕ, m_ϕ, p, T_0, and T_1, the primary variables w, u_ϕ, β_ϕ, Q, N_ϕ, and M_ϕ, and the secondary variables N_θ, M_θ, and Q_ϕ are typically

$$p_\phi = \sum_{n=0}^{P} p_{\phi n}(s,t)\cos n\theta + \sum_{n=1}^{P} \bar{p}_{\phi n}(s,t)\sin n\theta \tag{21}$$

The loadings p_θ and m_θ, the primary variables u_θ and N, and the secondary variables β_θ, $N_{\theta\phi}$, $M_{\theta\phi}$, and Q_θ are typically

$$p_\theta = \sum_{n=1}^{P} p_{\theta n}(s,t)\sin n\theta + \sum_{n=0}^{P} \bar{p}_{\theta n}(s,t)\cos n\theta \tag{22}$$

Upon substituting these Fourier series representations into our system of equations, we obtain $P+1$ separate decoupled systems of equations in the variables s and t to solve in lieu of the single system of equations in the variables θ, s, and t. For each system, we obtain two separate sets of equations—one set for the variables that are designated without a bar and another set for the variables designated with a bar. Here and elsewhere in the sequel where double signs occur in the equations, the upper sign is to accompany the first set of equations and the lower sign is to apply to the second set. Single signs will apply to both sets.

To facilitate writing the equations, we substitute the subscripted coefficients and loading terms A_1-A_{10}, B_1-B_{13}, C_1-C_9, and D_1-D_{50} for the more lengthy coefficients and loading terms in the equations. These quantities, which involve geometric and material parameters, loading terms, and the Fourier component designator n, are defined in Ref. 14.

With the aforementioned definition of coefficients and loading terms, our field equations for each Fourier harmonic are

$$-A_1 w_{n,sss} - A_2 w_{n,ss} + A_3 w_{n,s} + A_4 w_n + A_5 u_{\phi n,ss} + A_6 u_{\phi n,s} + A_7 u_{\phi n} \pm A_8 u_{\theta n,s} \pm A_9 u_{\theta n} - \frac{\gamma hr}{g} u_{\phi n,tt} = A_{10} - r\left(p_{\phi n} + \frac{1}{R_\phi} m_{\phi n}\right) \quad (23)$$

$$-B_1 w_{n,ssss} - B_2 w_{n,sss} + B_3 w_{n,ss} + B_4 w_{n,s} + B_5 w_n + B_6 u_{\phi n,sss} + B_7 u_{\phi n,ss} + B_8 u_{\phi n,s} + B_9 u_{\phi n} \pm B_{10} u_{\theta n,ss} \pm B_{11} u_{\theta n,s} \pm B_{12} u_{\theta n} - \frac{\gamma hr}{g} w_{n,tt} = B_{13} \mp n m_{\theta n} - r(p_n + m_{\phi n,s}) - m_{\phi n} \cos\phi \quad (24)$$

$$\pm C_1 w_{n,ss} \pm C_2 w_{n,s} \mp C_3 w_n \mp C_4 u_{\phi n,s} \mp C_5 u_{\phi n} + C_6 u_{\theta n,ss} + C_7 u_{\theta n,s} + C_8 u_{\theta n} - \frac{\gamma hr}{g} u_{\theta n,tt} = \mp C_9 - m_{\theta n} \sin\phi - r p_{\theta n} \quad (25)$$

The primary variables $\beta_{\phi n}$, Q_n, $N_{\phi n}$, N_n, and $M_{\phi n}$ are given by

$$\beta_{\phi n} = -w_{n,s} + \frac{1}{R_\phi} u_{\phi n} \quad (26)$$

$$Q_n = -D w_{n,sss} - D_{42} w_{n,ss} + D_{43} w_{n,s} - D_{44} w_n + D_{45} u_{\phi n,ss} + D_{46} u_{\phi n,s} + D_{47} u_{\phi n} \pm D_{48} u_{\theta n,s} \pm D_{49} u_{\theta n} - D_{50} + m_{\phi n} \quad (27)$$

$$N_{\phi n} = K(D_1 w_n + u_{\phi n,s} + D_2 u_{\phi n} \pm D_3 u_{\theta n} - D_4 T_{0n}) \quad (28)$$

$$N_n = \pm D_{37} w_{n,s} \mp D_{38} w_n \mp D_{39} u_{\phi n} + D_{40} u_{\theta n,s} + D_{41} u_{\theta n} \quad (29)$$

$$M_{\phi n} = D\left(-w_{n,ss} - {}_2 w_{n,s} + D_5 w_n + \frac{1}{R_\phi} u_{\phi n,s} + D_6 u_{\phi n} \pm D_7 u_{\theta n} - D_4 T_{1n}\right) \quad (30)$$

It will be convenient to also express the primary variables N_n and Q_n as

$$N_n = N_{\theta\phi n} + D_{36} M_{\theta\phi n} \quad (31)$$

$$Q_n = Q_{\phi n} \pm D_{10} M_{\theta\phi n} \quad (32)$$

The equations for the Fourier components of the secondary variables together with the details of the derivation of the governing equations for each Fourier harmonic may be found in Ref. 14.

Typical boundary conditions and the initial conditions for each Fourier harmonic are given by Eqs. (35) and (36), respectively, of Ref. 13.

Conversion of Equations to Finite-Difference Form

The equations to be solved for each Fourier harmonic consist of Eqs. (23-25) applied as the field equations, Eqs. (26-30) evaluated at each boundary, the equations for the boundary conditions, and the equations for the initial conditions. When this system of equations has been solved, the variables $\beta_{\phi n}$, $N_{\phi n}$, $M_{\phi n}$, N_n, and Q_n may be determined from Eqs. (26-30), respectively. To solve this system of equations, we replace all derivatives with their finite-difference equivalents to obtain a system of algebraic equations, which may be applied at successive increments of the time variable.

The accelerations at time t_1 are typically

$$\ddot{w}_n(s,t_1) = \{2[w_n(s,t_1) - w_n(s,t_0) - (\Delta t)\dot{w}_n(s,t_0)]\}/(\Delta t)^2 \quad (33)$$

For times $t \geq t_0 + 2\Delta t$ and $s_1 \leq s \leq s_{N-1}$, the accelerations will be given typically by

$$\ddot{w}_n(s,t-\Delta t) = [w_n(s,t-2\Delta t) - 2w_n(s,t-\Delta t) + w_n(s,t)]/(\Delta t)^2 \quad (34)$$

For times $t \geq t_0 + 2\Delta t$ and $s = s_0$ or $s = s_N$, the accelerations will typically be

$$\ddot{w}_n(s,t) = [w_n(s,t-2\Delta t) - 2w_n(s,t-\Delta t) + w_n(s,t)]/(\Delta t)^2 \quad (35)$$

To obtain convergent solutions for discontinuous distributed loadings, we have used an ordinary finite-difference representation for all spatial derivatives. By extending the meridional finite-difference mesh two additional node points beyond each of the boundaries s_0 and s_N, we also obtain the desired finite central difference representation for all derivatives on the interval $s_0 \leq s \leq s_N$. With this mesh we have $3N+25$ variables in our system of equations, where N is the number of equal increments along the meridian of the shell from s_0 to S_N; thus, to equalize the number of variables and the number of equations, we write Eqs. (23) and (25) at each of the node points s_{-1} and s_{N+1} in addition to writing the field equations (23-25) at all node points on the interval $s_0 \leq s \leq s_N$. For third derivatives at the points s_{-1} and s_{N+1}, we have used finite-difference representations, which are unbalanced about those pivotal points. Thus, our finite central difference representations are typically

$$w_{n,s}(s) = \frac{1}{2\Delta s}[-w_n(s-\Delta s) + w_n(s+\Delta s)] \quad (36)$$

$$w_{n,ss}(s) = \frac{1}{(\Delta s)^2}[w_n(s-\Delta s) - 2w_n(s) + w_n(s+\Delta s)] \quad (37)$$

$$w_{n,sss}(s) = \frac{1}{2(\Delta s)^3}[-w_n(s-2\Delta s) + 2w_n(s-\Delta s) - 2w_n(s+\Delta s) + w_n(s+2\Delta s)] \quad (38)$$

$$w_{n,ssss}(s) = \frac{1}{(\Delta s)^4}[w_n(s-2\Delta s) - 4w_n(s-\Delta s) + 6w_n(s) - 4w_n(s+\Delta s) + w_n(s+2\Delta s)] \quad (39)$$

Our third derivatives of w_n at the points s_{-1} and s_{N+1} are given by

$$w_{n,sss}(s_{-1}) = \frac{1}{2(\Delta s)^3}[-3w_n(s_{-2}) + 10w_n(s_{-1}) - 12w_n(s_0) + 6w_n(s_1) - w_n(s_2)] \quad (40)$$

$$w_{n,sss}(s_{N+1}) = \frac{1}{2(\Delta s)^3}[w_n(s_{N-2}) - 6w_n(s_{N-1}) + 12w_n(s_N) - 10w_n(s_{N+1}) + 3w_n(s_{N+2})] \quad (41)$$

To convert Eqs. (23-30) to spatial finite-difference form, we replace all derivatives by their representations given by Eqs. (36-41). Further, to produce more nearly equal coefficients in our equations, we define new force variables to be

$$N^0_{\phi n} = N_{\phi n} \times 10^{-6} \quad (42a)$$

$$M^0_{\phi n} = M_{\phi n} \times 10^{-6} \quad (42b)$$

$$N^0_n = N_n \times 10^{-6} \quad (42c)$$

$$Q^0_n = Q_n \times 10^{-6} \quad (42d)$$

and new coefficients C^0 of the force variables to be

$$C^0(N^0_{\phi n}) = C(N_{\phi n}) \times 10^6 \quad (43a)$$

$$C^0(M^0_{\phi n}) = C(M_{\phi n}) \times 10^6 \quad (43b)$$

$$C^0(N^0_n) = C(N_n) \times 10^6 \quad (43c)$$

$$C^0(Q^0_n) = C(Q_n) \times 10^6 \quad (43d)$$

By using Eq. (33) for the time derivatives together with the equations for the boundary conditions and the initial conditions, we obtain an implicit solution to our system of equations for the first time increment.

By using the accelerations given typically by Eq. (34) for the second and later time increments, we obtain explicit expressions for $w_n(s,t)$, $u_{\phi n}(s,t)$, and $u_{\phi n}(s,t)$ on the interval $s_1 \le s \le s_{N-1}$. After using these explicit expressions, we have 14 separate equations for each boundary available to evaluate implicitly the remaining variables for the time t. The fourteen equations for the boundary s_0 consist of Eqs. (26-30) written in finite-difference form and evaluated at s_0, Eqs. (23) and (25) written at s_{-1} and s_0, Eq. (24) written at s_0, and four equations specifying the boundary conditions. The 14 equations for the boundary S_N consist of Eqs. (26-30) evaluated at S_N, Eqs. (23) and (25) written at s_N and s_{N+1}, Eq. (24) written at s_N, and four equations defining the boundary conditions. The finite-difference equations for both t_1 and t may be found in Ref. 14.

Selection of Meridional and Time Increments

To solve the system of finite-difference equations, choices must be made for the increments Δs and Δt. These increments must have magnitudes that produce numerical stability of the finite-difference solution. A detailed discussion of the considerations involved and a description of the procedures used to select these increments may be found in Ref. 13. Briefly, the spatial increment Δs will be made sufficiently small to produce the desired accuracy for static solutions. To aid in the choice of time increment Δt, which is suitable to be used with the chosen spatial increment Δs, we use the Rayleigh-Ritz method to deterine the three lower frequencies of vibration of the shell for $n = 0$ and for the highest Fourier component n used to represent the loadings and dependent variables. We will then directly consider only the single Fourier component that has the highest calculated frequency ω_{max}. We will choose Δt to be some small fraction μ of the shortest calculated period from the relation

$$\Delta t = 2\mu\pi/\omega_{max} \quad (44)$$

where μ is a parameter to be designated upon the basis of experience with the differential equation formulation and finite-difference representations used. In regard to stability of the solution, we will choose Δt to be sufficiently small that, for two different values of Δt, the two solutions agree uniformly along the shell meridian at all corresponding times for the same increment Δs. Details of the determination of the three lower frequencies of vibration for the values of n are contained in Ref. 14.

Static Solutions for an Example Cylindrical Shell with Discontinuous Loading

Our finite-difference equations were programmed in FORTRAN IV, and all finite-difference values given here and subsequently for the typical solutions were obtained on a CDC 6600 computer.

To illustrate convergence of solutions of our system of equations for cases of discontinuous loadings, we have analyzed a cylindrical shell with the geometry shown in Fig. 4 when subjected to a discontinuous axisymmetric static loading of $p_0 = 4$ psi (27.58×10^3 Pa) applied between $s = 6.875$ and 7.125 in. (17.46-18.10 cm). For the boundary conditions, we assume that w, u_ϕ, u_θ, and M_ϕ are zero at s_0 and w, N_ϕ, u_θ, and M_ϕ are zero at s_N.

We assume a value of 30×10^6 psi (206×10^9 Pa) for E, a value of 0.284 lb/in.^{3} (0.786×10^{-2} kg/cm^3) for γ, and a

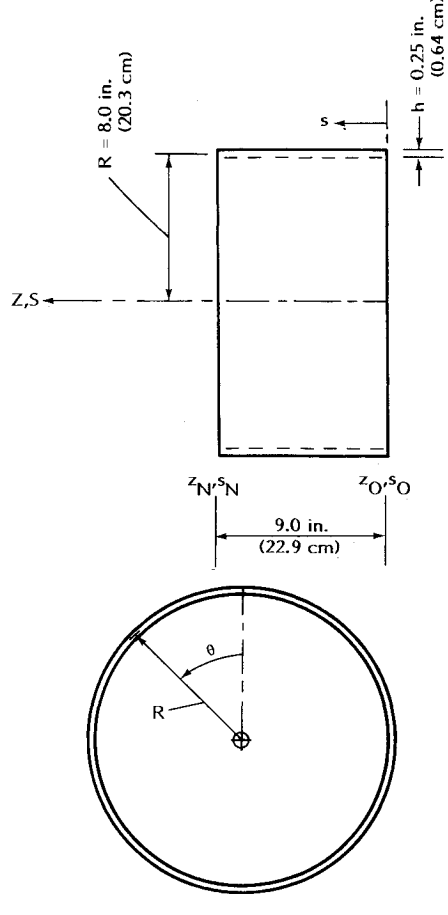

Fig. 4 Example cylindrical shell geometry.

Table 1 Example static solutions for cylindrical shell under axisymmetric discontinuous loading p_0

	$w(s)$, in.		
	Finite-difference solution		
s, in. (2.54 cm)	$\Delta s = 0.2500$ in. (0.64 cm)	$\Delta s = 0.0833$ in. (0.21 cm)	Exact solution
0.0	0.0	0.0	0.0
0.25	3.5593×10^{-10}	4.1359×10^{-10}	4.3574×10^{-10}
0.50	9.0189×10^{-11}	1.8896×10^{-10}	2.3058×10^{-10}
0.75	-1.4228×10^{-9}	-1.3164×10^{-9}	-1.2678×10^{-9}
1.00	-4.8101×10^{-9}	-4.7452×10^{-9}	-4.6834×10^{-9}
1.25	-1.0683×10^{-8}	-1.0723×10^{-8}	-1.0665×10^{-8}
1.50	-1.9605×10^{-8}	-1.9824×10^{-8}	-1.9780×10^{-8}
1.75	-3.2024×10^{-8}	-3.2501×10^{-8}	-3.2483×10^{-8}
2.00	-4.8179×10^{-8}	-4.8991×10^{-8}	-4.9010×10^{-8}
2.25	-6.7971×10^{-8}	-6.9180×10^{-8}	-6.9215×10^{-8}
2.50	-9.0787×10^{-8}	-9.2426×10^{-8}	-9.2543×10^{-8}
2.75	-1.1528×10^{-7}	-1.1734×10^{-7}	-1.1751×10^{-7}
3.00	-1.3917×10^{-7}	-1.4156×10^{-7}	-1.4178×10^{-7}
3.25	-1.5890×10^{-7}	-1.6146×10^{-7}	-1.6171×10^{-7}
3.50	-1.6946×10^{-7}	-1.7191×10^{-7}	-1.7217×10^{-7}
3.75	-1.6413×10^{-7}	-1.6609×10^{-7}	-1.6631×10^{-7}
4.00	-1.3438×10^{-7}	-1.3536×10^{-7}	-1.3549×10^{-7}
4.25	-6.9937×10^{-8}	-6.9354×10^{-8}	-6.9318×10^{-8}
4.50	4.0939×10^{-8}	4.3697×10^{-8}	4.3956×10^{-8}
4.75	2.1073×10^{-7}	2.1621×10^{-7}	2.1675×10^{-7}
5.00	4.5150×10^{-7}	4.6006×10^{-7}	4.6091×10^{-7}
5.25	7.7308×10^{-7}	7.8468×10^{-7}	7.8584×10^{-7}
5.50	1.1805×10^{-6}	1.1945×10^{-6}	1.1959×10^{-6}
5.75	1.6706×10^{-6}	1.6854×10^{-6}	1.6869×10^{-6}
6.00	2.2276×10^{-6}	2.2405×10^{-6}	2.2417×10^{-6}
6.25	2.8181×10^{-6}	2.8248×10^{-6}	2.8251×10^{-6}
6.50	3.3846×10^{-6}	3.3792×10^{-6}	3.3781×10^{-6}
6.75	3.8398×10^{-6}	3.8148×10^{-6}	3.8114×10^{-6}
7.00	4.0604×10^{-6}	4.0067×10^{-6}	4.0044×10^{-6}
7.25	3.8817×10^{-6}	3.8571×10^{-6}	3.8537×10^{-6}
7.50	3.4599×10^{-6}	3.4552×10^{-6}	3.4542×10^{-6}
7.75	2.9096×10^{-6}	2.9168×10^{-6}	2.9173×10^{-6}
8.00	2.3086×10^{-6}	2.3214×10^{-6}	2.3226×10^{-6}
8.25	1.7035×10^{-6}	1.7170×10^{-6}	1.7184×10^{-6}
8.50	1.1164×10^{-6}	1.1272×10^{-6}	1.1284×10^{-6}
8.75	5.5130×10^{-7}	5.5720×10^{-7}	5.5783×10^{-7}
9.00	0.0	0.0	0.0

value of 0.30 for ν. We obtain our static solutions for both 36 equal meridional increments and 108 equal meridional increments between s_0 and s_N by setting the time increment Δt equal to infinity and solving for time t_1 the system of equations developed in Ref. 14.

Table 1 depicts the nodal point displacements w as obtained by the ordinary finite-difference method and as obtained exactly by closed-form solution of the fourth-order differential equation for cylindrical shells after evaluation of the internal shell forces at the points of loading discontinuities by the classical method of indeterminate structures. It can be seen in Table 1 that the ordinary finite-difference solutions are in very close agreement with the exact solution and that, in general, the solutions converge more closely to the exact solution through use of the smaller values for Δs.

Static Solutions for Example Parabolic Shell with Discontinuous Loading

As a second example, we include the static analysis of the parabolic shell with the geometry and discontinuous loading shown in Fig. 5. For the boundary conditions, we assume that w, u_ϕ, u_θ, and β_ϕ are zero at s_0 and Q, N_ϕ, N, and M_ϕ are zero at s_N. We use a value of 30×10^6 psi (206×10^9 Pa) for E, a value of 0.284 lb/in.^{3} (0.786×10^{-2} kg/cm^3) for γ, and a value of 0.30 for ν.

Table 2 Example finite-difference solutions in local shell coordinates at $\theta = 0$ for parabolic shell with discontinuous loading p

s, in.	z, in.	w, in.	u_ϕ, in.
0.00	0.00	0.0	0.0
0.46	0.45	-3.581×10^{-4}	7.901×10^{-4}
0.92	0.91	-1.418×10^{-3}	1.530×10^{-3}
1.70	1.67	-4.165×10^{-3}	2.642×10^{-3}
2.62	2.57	-8.009×10^{-3}	3.770×10^{-3}
3.55	3.47	-1.190×10^{-2}	4.675×10^{-3}
4.63	4.50	-1.648×10^{-2}	5.462×10^{-3}
5.71	5.52	-2.116×10^{-2}	5.975×10^{-3}
6.80	6.53	-2.600×10^{-2}	6.231×10^{-3}
7.88	7.52	-3.100×10^{-2}	6.247×10^{-3}
8.96	8.50	-3.617×10^{-2}	6.039×10^{-3}
10.04	9.46	-4.133×10^{-2}	5.628×10^{-3}
11.28	10.55	-4.626×10^{-2}	4.938×10^{-3}
12.36	11.48	-4.915×10^{-2}	4.181×10^{-3}
13.60	12.53	-5.761×10^{-2}	3.168×10^{-3}
14.83	13.55	-9.497×10^{-2}	1.879×10^{-3}
15.45	14.06	-1.270×10^{-1}	1.033×10^{-3}
15.53	14.12	-1.309×10^{-1}	9.142×10^{-4}
15.61	14.18	-1.348×10^{-1}	7.952×10^{-4}
15.92	14.43	-1.475×10^{-1}	2.896×10^{-4}
16.69	15.06	-1.521×10^{-1}	-1.081×10^{-3}
17.00	15.30	-1.428×10^{-1}	-1.636×10^{-3}
17.08	15.36	-1.397×10^{-1}	-1.772×10^{-3}
17.15	15.42	-1.366×10^{-1}	-1.908×10^{-3}
17.92	16.03	-1.037×10^{-1}	-3.195×10^{-3}
19.16	16.99	-7.629×10^{-2}	-5.015×10^{-3}
20.55	18.05	-7.494×10^{-2}	-6.901×10^{-3}
21.79	18.98	-7.997×10^{-2}	-8.535×10^{-3}
23.18	20.00	-8.537×10^{-2}	-1.034×10^{-2}

For the given conditions, only the equations containing the symmetric Fourier components enter into the solution. We consider only the Fourier components for $n = 0$–8 and use $p_0 = -318$, $p_1 = -500$, $p_2 = -212$, $p_4 = 42$, $p_6 = -18$, and $p_8 = 10$ psi (-2192×10^3, -3447×10^3, -1462×10^3, 290×10^3, -124×10^3, and 69×10^3 Pa) for the six nonzero components of loading. We obtain our static solution in the local shell coordinate system for the six Fourier components of loading by specifying 150 equal increments Δs along the meridian from s_0 to s_N, setting the time increment Δt equal to infinity, and solving for time t_1 the system of equations given in Ref. 14. With an arc length s between s_0 and s_N computed in the program to be approximately 23.18 in. (58.89 cm), our value used for Δs is thus approximately 0.1545 in. (0.39 cm).

Table 2 shows the displacements w and u_ϕ in the local shell coordinate system at selected node points along the meridian $\theta = 0$. We show also values of w and u_ϕ on the meridian $\theta = 0$ for the values of s at which the loading is discontinuous, as shown in Fig. 5. These latter values are obtained by linear interpolation between the values at the two adjacent finite-difference node points in each case.

For comparison purposes, we have obtained, by use of the finite-element program COSMOS 7, the static solution for the parabolic shell with the geometry shown in Fig. 5 when subjected to the same boundary conditions and six Fourier components of loading used in the finite-difference solution described previously. Due to symmetry of geometry and loading, the finite-element grid was formed for the region $0 \le \theta \le \pi$ and $s_0 \le s \le s_N$ only. This region was modeled with 648 isoparametric doubly curved 9-node thin-shell elements consisting of 24 equally spaced elements in the direction of θ and 27 variably spaced elements in the direction of s. Elements were more closely spaced meridionally adjacent to the free boundary at s_N and in the vicinity of the loading to provide optimum modeling of the shell structure.

The solution for the global displacements ΔX, ΔY, and ΔZ by use of the COSMOS 7 program was obtained in the global coordinate system XYZ as shown in Fig. 5. To com-

Table 3 Example global coordinate finite-difference and finite-element solutions at $\theta = 0$ for parabolic shell with discontinuous loading p

	Finite-difference solution		COSMOS 7 finite-element solution	
s, in.	Y, in.	Z, in.	Y, in.	Z, in.
0.00	0.0	0.0	0.0	0.0
0.46	-2.219×10^{-4}	8.385×10^{-4}	-2.192×10^{-4}	8.345×10^{-4}
0.92	-1.113×10^{-3}	1.764×10^{-3}	-1.170×10^{-3}	1.769×10^{-3}
1.70	-3.510×10^{-3}	3.465×10^{-3}	-3.651×10^{-3}	3.490×10^{-3}
2.62	-6.840×10^{-3}	5.619×10^{-3}	-6.944×10^{-3}	5.638×10^{-3}
3.55	-1.014×10^{-2}	7.794×10^{-3}	-1.033×10^{-2}	7.843×10^{-3}
4.63	-1.394×10^{-2}	1.035×10^{-2}	-1.400×10^{-2}	1.036×10^{-2}
5.71	-1.776×10^{-2}	1.296×10^{-2}	-1.779×10^{-2}	1.296×10^{-2}
6.80	-2.168×10^{-2}	1.565×10^{-2}	-2.178×10^{-2}	1.568×10^{-2}
7.88	-2.569×10^{-2}	1.844×10^{-2}	-2.575×10^{-2}	1.845×10^{-2}
8.96	-2.982×10^{-2}	2.134×10^{-2}	-2.994×10^{-2}	2.139×10^{-2}
10.04	-3.391×10^{-2}	2.429×10^{-2}	-3.408×10^{-2}	2.437×10^{-2}
11.28	-3.770×10^{-2}	2.726×10^{-2}	-3.790×10^{-2}	2.735×10^{-2}
12.36	-3.980×10^{-2}	2.915×10^{-2}	-3.998×10^{-2}	2.924×10^{-2}
13.60	-4.655×10^{-2}	3.409×10^{-2}	-4.683×10^{-2}	3.421×10^{-2}
14.83	-7.702×10^{-2}	5.560×10^{-2}	-7.744×10^{-2}	5.566×10^{-2}
15.45	-1.028×10^{-1}	7.453×10^{-2}	-1.030×10^{-1}	7.448×10^{-2}
15.53	-1.059×10^{-1}	7.688×10^{-2}	-1.062×10^{-1}	7.687×10^{-2}
15.61	-1.091×10^{-1}	7.923×10^{-2}	-1.088×10^{-1}	7.886×10^{-2}
15.92	-1.191×10^{-1}	8.701×10^{-2}	-1.191×10^{-1}	8.683×10^{-2}
16.69	-1.222×10^{-1}	9.058×10^{-2}	-1.221×10^{-1}	9.032×10^{-2}
17.00	-1.146×10^{-1}	8.527×10^{-2}	-1.142×10^{-1}	8.476×10^{-2}
17.08	-1.120×10^{-1}	8.345×10^{-2}	-1.122×10^{-1}	8.337×10^{-3}
17.15	-1.095×10^{-1}	8.163×10^{-2}	-1.093×10^{-1}	8.117×10^{-2}
17.92	-8.329×10^{-2}	6.168×10^{-2}	-8.347×10^{-2}	6.173×10^{-2}
19.16	-6.191×10^{-2}	4.486×10^{-2}	-6.202×10^{-2}	4.467×10^{-2}
20.55	-6.101×10^{-2}	4.406×10^{-2}	-6.104×10^{-2}	4.379×10^{-2}
21.79	-6.491×10^{-2}	4.748×10^{-2}	-6.488×10^{-2}	4.716×10^{-2}
23.18	-6.902×10^{-2}	5.130×10^{-2}	-6.892×10^{-2}	5.090×10^{-2}

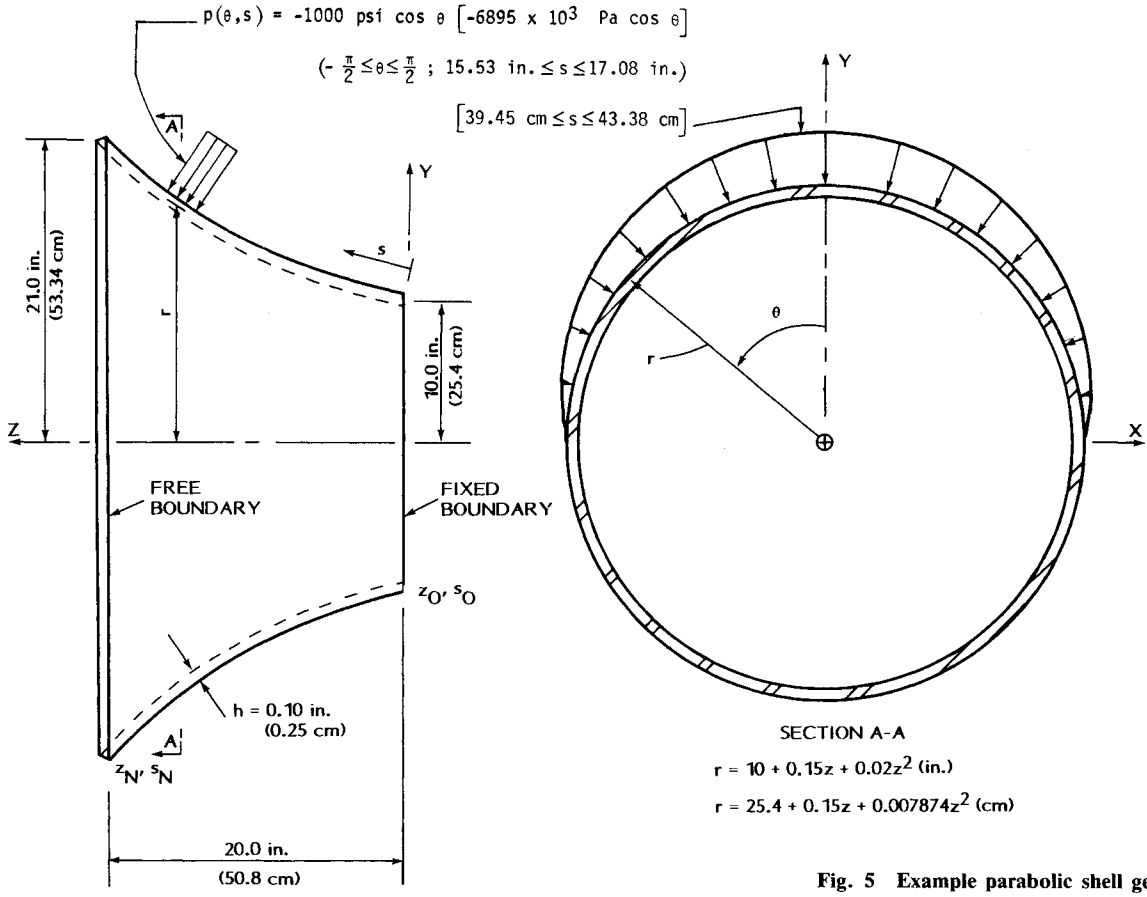

Fig. 5 Example parabolic shell geometry and loading.

pare the finite-difference solution with the COSMOS 7 finite-element solution thus obtained, we transform the finite-difference solution given in Table 2 in the local shell coordinate system to the XYZ global coordinate system and show both solutions in the global coordinate system in Table 3. It may be seen by study of Table 3 that the finite-difference solution is at all points, including the boundaries and points of loading discontinuities, in very close agreement with the COSMOS 7 finite-element solution.

Convergence of Solution Considerations

The system of finite-difference equations contained herein utilizes an ordinary finite-difference representation of the derivatives in conjunction with the displacement formulation of the governing differential equations. We have shown by application of this system of equations to the solution for typical cases of discontinuous loadings applied to typical cylindrical, conical, spherical, elliptical, and parabolic shells that the solutions converge to the correct solutions without segmenting the shell at points of loading discontinuities. Examples of this convergence have been given for a cylindrical shell in Table 1 and for a parabolic shell in Table 3. On the other hand, numerical results found for typical shells under discontinuous loadings with the use of the displacement formulation of the equations and higher-order finite-difference representations as used in Ref. 13 demonstrate that convergence to the correct solution cannot be obtained without segmenting the shell at points of loading discontinuities. Similar numerical results show that, for discontinuous loadings, convergence to the correct solution cannot be obtained by the representations used in Refs. 6 and 16, both of which use eight first-order differential equations as the field equations together with ordinary and higher-order finite-difference representations for the derivatives, respectively, without segmenting the shell at points of loading discontinuities. It is seen from these numerical results that convergence of the finite-difference solution to the correct solution for shells under discontinuous distributed loadings without segmenting the shell is dependent upon both the formulation of the governing differential equations and the finite-difference representations used for the derivatives.

In general, we expect correctly converging solutions for discontinuous loadings without segmenting the shell at points of loading discontinuities if derivatives no higher than those appearing in the field equations appear in the Taylor series expansions for the finite-difference representations for the derivatives. For the displacement formulation of the differential equations and the ordinary finite-difference representations used herein, this condition is satisfied with the exception of the use of $u_{\phi,ssss}$ in the Taylor series expansion for $u_{\phi,sss}$ (the highest derivative of u_ϕ occurring in the field equations). Nonetheless, since both $u_{\phi,sss}$ and $u_{\phi,ssss}$ are represented by the same expanse of nodal points in the finite-difference representations, we expect no extraneous roots due to the use of $u_{\phi,ssss}$ in the Taylor series expansion. Thus, since the equilibrium equations are also never written at points of loading jump discontinuities, we expect our solutions to converge to the correct solutions.

Similarly, in those cases for which the Taylor series expansions for all derivatives in the field equations contain derivatives higher than those in the field equations, we do not expect correctly converging solutions for discontinuous loadings without segmenting the shell at points of loading discontinuities. Thus, if we use the displacement formulation of the differential equations in conjunction with a higher-order finite-difference representation of the derivatives, as in Ref. 13, derivatives two orders higher than those appearing in the equilibrim equations appear in the Taylor series expansions for the finite-difference representations for the derivatives. These higher-order derivatives would remain undefined by the equilibrium equations. Also, if we use an eight first-order differential equation formulation of the field differential equations together with either an ordinary finite central difference representation of the first derivatives in the field equations as in Ref. 6 or with a higher-order finite central difference representation of the first derivatives as in Ref. 16, derivatives higher than those in the field equations again appear in the Taylor series expansions for all finite-difference representations for the derivatives. Again, lack of definition of these higher-order derivatives by use of the field equations leads us to expect solutions that fail to converge to the correct solutions for discontinuous loadings without segmenting the shell at points of loading discontinuities.

The numerical results and considerations described herein demonstrate convergence and correctness of solutions for discontinuous distributed loadings by use of the loading representations, differential equation formulation, and finite-difference representations used herein without segmenting the shell at points of loading discontinuities.

Conclusions

The results shown in Tables 1 and 3 for the typical examples, together with numerical results not shown, indicate that the ordinary spatial finite-difference representations used in conjunction with the displacement formulation of the differential equations as given herein yield converging and correct solutions for any general continuous or discontinuous loading discontinuities. The formulation thus constitutes an expeditious procedure for either the static or dynamic response analysis of rotationally symmetric variable thickness general shells under general loadings.

Acknowledgment

Grateful acknowledgment is extended to Mr. John W. Sofferis, Systems Simulation and Development Directorate, U.S. Army Missile Command, Redstone Arsenal, AL, who modeled the finite-element grid and obtained the finite-element computer program COSMOS 7 solution for the parabolic shell and loading shown in Fig. 5.

References

[1]Penny, R. K., "Symmetric Bending of the General Shell of Revolution by Finite Difference Methods," *Journal of Mechanical Engineering Science*, Vol. 3, No. 4, Dec. 1961, pp. 369–377.

[2]Radkowski, P. P., Davis, R. M., and Bolduc, M. R., "Numerical Analysis of Equations of Thin Shells of Revolution," *ARS Journal*, Vol. 32, Jan. 1962, pp. 36–41.

[3]Budiansky, B. and Radkowski, P. P., "Numerical Analysis of Unsymmetrical Bending of Shells of Revolution," *AIAA Journal*, Vol. 1, Aug. 1963, pp. 1833–1842.

[4]Johnson, D. E. and Greif, R., "Dynamic Response of a Cylindrical Shell: Two Numerical Methods," *AIAA Journal*, Vol. 4, March 1966, pp. 486–494.

[5]Bushnell, D., "Analysis of Buckling and Vibration of Ring-Stiffened, Segmented Shells of Revolution," *International Journal of Solids and Structures*, Vol. 6, Jan. 1970, pp. 157–181.

[6]Smith, T. A., "Numerical Analysis of Rotationally Symmetric Shells Under Transient Loadings," *AIAA Journal*, Vol. 9, April 1971, pp. 637–643.

[7]Greenbaum, G. A. and Cappelli, A. P., "The Numerical Methods of Discrete Shell Analysis." *Computer Oriented Analysis of Shell Structures,* edited by R. F. Hartung, AFFDL-TR-71-79, June 1971, pp. 34–64.

[8]Anderson, M. S., Fulton, R. E., Heard, W. L., Jr., and Walz, J. E., "Stress, Buckling, and Vibration Analysis of Shells of Revolution," *Computers and Structures,* Vol. 1, Nos. 1/2, Aug. 1971, pp. 157–192.

[9]Noor, A. K. and Stephens, W. B., *Comparison of Finite-Difference Schemes for Analysis of Shells of Revolution,* NASA TN-D-7337, Dec. 1973.

[10]Bushnell, D., "Finite-Difference Energy Models Versus Finite Element Models: Two Variational Approaches in One Computer Program," *Numerical and Computer Methods in Structural*

Mechanics, edited by S. J. Fenves, N. Perrone, A. R. Robinson, and W. C. Schnobrich, Academic Press, New York, 1973, pp. 291-336.

[11]Bushnell, D., "BOSOR-5—Program for Buckling of Elastic-Plastic Complex Shells of Revolution Including Large Deflections and Creep," *Computers and Structures*, Vol. 6, 1976, pp. 221-239.

[12]Bushnell, D., "BOSOR-4—Program for Stress, Buckling, and Vibration of Complex Shells of Revolution," *Structural Mechanics Software Series*, Vol. 1, edited by N. Perrone and W. Pilkey, University Press of Virginia, Charlottesville, VA, 1977, pp. 11-143.

[13]Smith, T. A., "Explicit High-Order Finite-Difference Analysis of Rotationally Symmetric Shells," *AIAA Journal*, Vol. 18, March 1980, pp. 309-317.

[14]Smith, T. A., "Finite Difference Analysis of Rotationally Symmetric Shells Under Discontinuous Distributed Loadings," TR RL-83-5, U.S. Army Missile Command, Redstone Arsenal, AL, July 1983.

[15]Reissner, E., "A New Derivation of the Equations for the Deformation of Elastic Shells," *American Journal of Mathematics*, Vol. 63, 1941, pp. 177-184.

[16]Smith, T. A., "Implicit High Order Finite Difference Analysis of Rotationally Symmetric Shells," RL-73-9, U. S. Army Missile Command, Redstone Arsenal, AL, Oct. 15, 1973.